Biochemical and Biophysical Research Communications **279,** 265–269 (2000)
doi:10.1006/bbrc.2000.3943, available online at http://www.idealibrary.com on IDEAL®

Oligonucleotide-Capped Gold Nanoparticles for Improved Atomic Force Microscopic Imaging and Enhanced Selectivity in Polynucleotide Detection

Shubo Han, Jianqiao Lin, Feimeng Zhou,[1] and Robert Luis Vellanoweth
Department of Chemistry and Biochemistry, California State University at Los Angeles, Los Angeles, California 90032

Received November 2, 2000

A novel assay for selective determination of polynucleotides using atomic force microscopy in conjunction with the formation of the probe/target/DNA–gold nanoparticle sandwich structure at a gold surface is described. A 17-mer probe was attached to the surface for subsequent hybridization with a polynucleotide target. Due to the flat orientation of the probe–target hybrid with respect to the surface and the spatial obstruction of the unhybridized probes near the hybrids, the AFM images are not clear. The hybridization efficiency was estimated to be about 1.1% since certain surface features could not be resolved. The utilization of 30-mer-capped gold nanoparticles not only provides another dimension of selectivity, but also reorients the previously formed probe–target hybrid in such a way that the strands of the target become tethered with respect to the surface. This reorientation improves the resolution in imaging the hybridized target molecules and provides an accurate determination of the hybridization efficiency (16%).

Key Words: **DNA sensing; atomic force microscope; gold nanoparticles; DNA surface orientation.**

Sequence-specific DNA assays of target nucleic acids by hybridization with DNA probes at a solid/solution interface (heterogeneous DNA sensors) are an important avenue for detecting DNA samples of biological origins (1, 2). In the past few years, the use of thiolated oligonucleotides immobilized onto gold surfaces has received a considerable amount of attention (3–8), due in part to the control and flexibility in forming self-assembled monolayers (SAMs) of DNA and/or mixed DNA/alkanethiol SAMs. Thiolated DNA probes have also been immobilized onto thin gold films for gravimetric analysis (9, 10), electrochemical detection (11, 12), and AFM imaging of DNA targets (5, 13, 14). More recently, several rapid, sensitive, and selective DNA detection methods using gold nanoparticles covered with oligonucleotides have been developed by Mirkin, Letsinger and their co-workers (15–21). In addition to the fundamental interest and potential applications associated with these systems (3, 4, 6–8, 14, 22–24), the formation of well-ordered DNA films and nanoparticle networks has also enhanced the selectivity and sensitivity of other types of DNA detection schemes. For example, oligonucleotide-capped gold nanoparticles have been shown to improve the sensitivity of techniques such as quartz crystal microbalance (25, 26) and surface plasmon resonance (27) for the detection of DNA hybridization. Recently, a comparison of gold films and nanoparticles for the attachment of thiolated oligonucleotides and for the subsequent DNA hybridization has been made by Demers *et al.* (15)

We report here the use of a probe/target/DNA-nanoparticle sandwich structure in conjunction with AFM imaging for the detection of hybridization of large polynucleotide targets (M13 phage DNA) across a small and highly localized surface. AFM has been demonstrated to be a powerful and sensitive method for detecting surface-confined DNA molecules at molecular levels (28, 29). The employment of DNA-capped gold nanoparticles in this procedure caused a somewhat unexpected rearrangement of the surface-confined probe–target hybrids and the rearrangement significantly enhanced the quality of AFM imaging. As a consequence, the hybridized target molecules become easily discernable at the microscopic level and the DNA hybridization efficiency can be accurately determined. The oligonucleotide present on the gold nanoparticles provides another dimension of specificity which enabled us to distinguish polynucleotides of very similar sizes and base sequences (M13 mp18(+) vs M13 mp19(+)). The reorientation of the probe–target hybrid by the gold nanoparticle is explained on the basis of steric hindrance and electrostatic interaction with the adjacent probe molecules. We also carried out contact angle measurements in an attempt to under-

[1] To whom correspondence should be addressed.

0006-291X/00 $35.00

stand the surface structures of the various DNA-covered gold surfaces at the macroscopic level.

EXPERIMENTAL

Materials

EDTA and Tris · HCl were both from Sigma (St. Louis, MO). Hydrogen tetracholoroaurate(III) hydrate and sodium citrate were obtained from Aldrich Chemicals (Milwaukee, WI). M13mp18(+) and M13mp19(+) ss-phage DNA were purchased from Amersham Pharmacia Biotech (Piscataway, NJ) and Life Technologies (Rockville, MD), respectively. M13 phage DNA has 7249 bases and the strand length should be around 2.46 μm if 0.34 nm is used as the base spacing. But this value is probably an overestimate since the 0.34 nm spacing is for less flexible double-stranded DNA. The thiolated 17-mer probe, SH-$(CH_2)_6$-5′-GTAAAACGACGGCCAGT-3′ and the thiolated 30-mer 5′-AGAGGATCCCCGGGTACCGAGCTCGAATTC-3′-$(CH_2)_3$SH were both acquired from IDT Inc. (Coralville, IA). The 17mer is selective to both targets since the hybridization occurs outside of the multiple-cloning site, but the 30-mer, immobilized onto gold nanoparticles, is only selective to the multiple cloning site of M13mp18(+). The site on the M13mp18(+) that is complementary to the 17-mer is 31 bases away from the multiple cloning site. Gold (111) evaporated on mica were used as the substrate for AFM imaging.

Procedures

(a) Solution preparation. The DNA probe stock solutions were prepared in Tris · HCl/EDTA (TE) buffer solutions (10 mM Tris · HCl and 1 mM EDTA) inside a glove box (Plas Labs, Lansing, Mich.). Dilute probe solutions were prepared daily using aliquots pipetted from the stock solution inside the glove box. Target M13 phage DNA solutions were prepared with 10 mM Tris–HCl/0.1 M NaCl (TNE) buffer. The synthesis of gold nanoparticles follows the literature procedure (30, 31), and the size (13 nm in diameter) of these nanoparticles was confirmed with UV–visible spectrometry. The DNA-capped gold nanoparticles were prepared by reacting 5.5 mL of 17 nM gold nanoparticles with 12 mM 30-mer oligonucleotide. After 16 h, the solution was brought TNE solution and allowed to stand for 40 h. This was followed by centrifugation for at least 25 min to remove excess regents. The red oily precipitate was then washed twice with the Tris–HCl/NaCl solution.

(b) Atomic force microscope experiments. The AFM instrument and operational conditions have been described elsewhere (14). Gold substrates were first soaked in 0.5 μM 17-mer DNA for 4 h at room temperature in the glove box. This was followed by exposing the probe-modified substrate to 6.7 μg/mL target DNA in TNE for 30 min. Prior to AFM imaging, the DNA-covered gold substrate was rinsed with deionized water. The AFM images were then collected in a liquid cell which contained a TNE solution. For experiments that involved the use of the DNA-capped gold nanoparticles, the gold substrate covered with both probe and target DNA molecules was immersed in a 94 nM 30-mer-capped gold nanoparticle solution for 2 h. After thorough rinsing with water, the film was imaged in the TNE solution.

(c) Contact angle measurements. Contact angles at bare gold substrate and gold surfaces covered with DNA molecules and DNA/nanoparticles were measured using a Cam-Plus Microcontact angle meter (KSV Instruments, Monroe, CT). Contact angle measurements and AFM imaging experiments were performed concomitantly at the same substrate in order to provide a one-to-one comparison during data interpretation.

RESULTS AND DISCUSSION

Figure 1 illustrates a simplified schematic of the three-step procedure that improves AFM imaging of

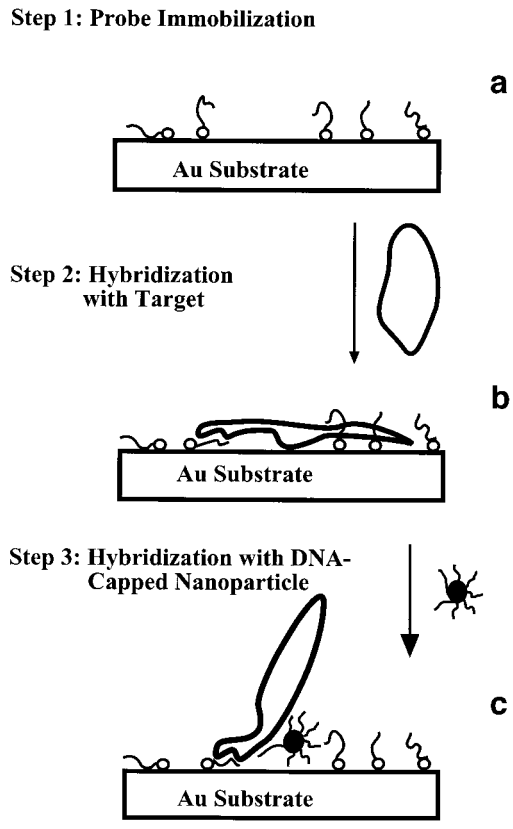

FIG. 1. Schematic representation of the procedure employed in the assay for the probe immobilization (Step 1), hybridization of the M13 phage target DNA (Step 2), and the second hybridization utilizing oligonucleotide-capped gold nanoparticles (Step 3). The diagram is not drawn to the scale but the orientations of the probe, the hybrid, and the hybrid with the second probe attached to the nanoparticle are depicted according to the published results and observations in this work. The empty circles represent the thiol tether groups.

polynucleotides. This procedure also provides an opportunity for an additional discrimination of polynucleotide targets of similar size and base sequence. In Step 1, the immobilization of thiolated oligonucleotides produces a DNA film whose coverage and molecular orientations have been well studied by other researchers (3, 4, 7, 8, 22) as well as in our previous AFM work (32). Tarlov and co-workers showed this model to represent the possible arrangements of thiolated DNA at gold surfaces (3, 22). They also demonstrated experimentally that the DNA film is not as compact as that of a regular alkanethiol and the DNA orientation is somewhat random due to the interaction between the DNA bases and the gold surface. In Step 2, the M13 phage DNA target was hybridized by the surface-confined oligonucleotide probes. As revealed in our previous AFM work and confirmed again in the images shown below, the hybrids tend to adopt exclusively an orientation in which the DNA coil(s) are parallel to the underlying substrate (14). We have shown that the

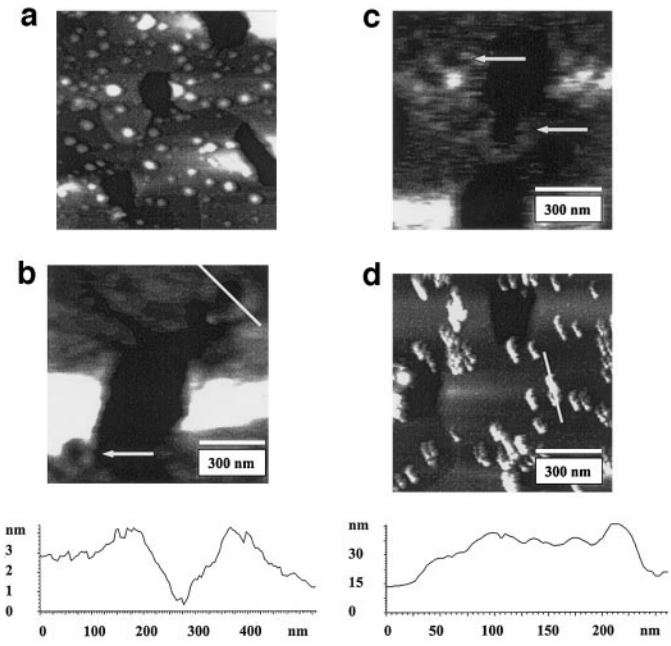

FIG. 2. Topographic MAC-AFM images of (a) a Au(111) substrate modified with thiolated 17-mer probes; (b) a probe-covered Au(111) substrate upon exposure to a 6.7 μg/mL M13mp18(+) solution; (c) a probe-modified Au(111) substrate upon hybridization in a 6.7 μg/mL M13mp19(+) solution; and (d) the surface in (b) after being immersed in a 30-mer-capped Au nanoparticle solution. In b and d, the cross-sectional contours correspond to the white bars across the respective features.

hybridization efficiency between the probe and the polynucleotide is far below that observed between the probe and an oligonucleotide target. Because of this orientation, the hybrids were "buried" underneath the rambling strands of unhybridized probes. Such a configuration renders difficulty to AFM experiments as the imaging relies on the interaction of the AFM tip with surface features without severe obstruction (28, 33, 34). As will be seen below in the description of our AFM images, the use of DNA-capped gold nanoparticles helps resolve this problem. The use of such nanoparticles, with the DNA caps having a sequence complementary to a different portion of the polynucleotide, causes the DNA coil(s) to tilt with respect to the substrate. As a consequence, a major portion of the hybrid DNA strand protrudes above the short unhybridized probe molecules.

Figure 2 shows a series of AFM images obtained upon different DNA immobilization and hybridization reactions. Shown in Fig. 2a is a representative image of a gold substrate modified with the thiolated DNA probe. The size and distribution of the oligonucleotides agree well with those of our previous study, with the dots having an average diameter of about 26–40 nm and a surface density of about 1.1×10^{10} molecules/cm^2. The average height of the probe is about 4–10 nm which is in close agreement with the theoretical value expected from a 17-mer (about 6 nm). The spacing between two neighboring probes is typically around 20–50 nm, which is almost two orders of magnitude wider than that expected from the $(\sqrt{3} \times \sqrt{3})R30^0$ packing of a typical alkanethiol (The nearest spacing is 0.5 nm) (35). A typical AFM image of the surface upon hybridization in a M13 mp18(+) target solution is displayed in Fig. 2b. As can been seen, many circular structures are vaguely discernable. These circles have an average length of 0.7–1.2 μm and a width of about 30–50 nm. The strand width observed by AFM is typically around 13 $\pm$ 2 nm from various AFM studies of DNA (13, 28, 29). The somewhat greater strand width found here is mainly ascribed to the uncertainty in obtaining a value from the relatively blurry images of these circular structures. It is therefore apparent that the position of the "buried" polynucleotide relative to the tethered unhybridized probe molecules is not favorable for AFM imaging. It is also worth mentioning that the height of these circles, deduced from the cross-sectional contours, is about 2 nm. Such a value is in close to the theoretical strand width of DNA molecules (36). Owing to the flat orientation and the obstruction arising from the adjacent unhybridized probe molecules, it is difficult to deduce the exact number of the circular DNA molecules with AFM. While Fig. 2b qualitatively proves that hybridization does take place, there is a large uncertainty in the estimation of the hybridization efficiency. When we count only the resolvable circles and treat them as the possible oligonucleotide-polynucleotide complexes, the surface density of the hybrid DNA molecules was found to be about 1.2×10^8 molecules/cm^2. Thus the hybridization efficiency appears to be around only 1.1% (calculated by dividing the surface density of the hybrids by that of the probes deduced from Fig. 2a).

Utilizing the same DNA probes immobilized on the gold surface (in Step 1), M13 mp19(+) was also found to be hybridizable and the resultant AFM image is shown in Fig. 2c. A comparison between Figs. 2b and 2c indicates that both surfaces are similar. This is not surprising since the probe has a sequence that is also complementary to M13 mp19(+) and both types of targets are very similar in terms of their structures and base sequences. As expected, the probe binds effectively to both polynucleotide targets.

As mentioned in connection with the description of the procedure, we carried out an additional analysis by using gold nanoparticles covered with a 30-mer whose sequence is complementary only to the multiple cloning site of the M13 mp18(+). While the AFM image of the surface in Fig. 2c remained essentially unchanged after being exposed to the DNA-capped gold nanoparticle solution for 2 h (not shown), the AFM image of the surface represented by Fig. 2b was significantly different. As shown in Fig. 2d, many oblong objects appear upon the implementation of Step 3 in Fig. 1. Close

examinations of some of these objects reveal that they resemble circles tethering to the surface with a small tilt angle with respect to the surface normal. These features have an average length of 0.68 μm and a height of 20–25 nm. In deducing the length, we assume that the topmost portion of the polynucleotide coil imaged has the same length of the underlying portion (i.e., 0.34 μm $\times$ 2 = 0.68 μm) and the total height is 0.05 μm (2 $\times$ 0.025 μm). Therefore, the total strand length of the target was crudely estimated to be about 0.73 μm. This value is somewhat shorter than the perimeter of the target estimated from Fig. 2b (0.7–1.2 μm). It is worth mentioning that the height of the polynucleotide coil, though much longer than the probe (4–10 nm), does not reflect accurately the actual height. This is because circular single-stranded polynucleotides are flexible molecules and the height can be significantly reduced when the AFM tip scans over and compresses the polynucleotide coil. Given the uncertainty associated with the estimation of the height, 0.73 μm is still close to the lower limit of the perimeter range estimated from Fig. 2b.

Although the experiment using a target whose sequence is not complementary to the probe sequence on the nanoparticles suggests that the features in Fig. 2d must have originated from the second hybridization event (Step 3 in Fig. 1), we carried out another control experiment to verify that oligonucleotide-capped gold nanoparticles do not adhere to the probe-covered surface. The image (not shown) acquired at a 17-mer-covered surface, upon being immersed in an oligonucleotide-covered nanoparticle solution for 2 h, is essentially the same as that in Fig. 2a. Therefore, we are confident that only a legitimate hybridization between the oligonucleotide-capped nanoparticles and the surface-confined target molecules will produce images like that in Fig. 2d.

The comparison between Figs. 2b and 2d clearly demonstrates that the reorientation of the sandwich structure drastically improves the resolution of the hybridized target molecules. The unambiguous counting of the tethered hybrids enabled us to measure the hybridization efficiency (16%) accurately. Obviously, the hybridization efficiency deduced from Fig. 2b is a gross underestimate.

The spatial rearrangement of the polynucleotide target between Figs. 2b and 2d can be reasoned on the basis of the aforementioned necessity for reducing steric hindrance and electrostatic repulsion. Recall that the spacing between the 17-mer probes is typically around 20–50 nm (Fig. 2a) and the DNA capped gold nanoparticles have a diameter of about 33 nm (diameter of gold nanoparticle (13 nm) + 2 $\times$ the length of the 30-mer ($\sim$10 nm)). Thus, the incorporation of the 30-mer-capped gold nanoparticle into the probe–polynucleotide hybrid would make the hybrid experience a much greater repulsion from the negatively charged unhybridized probes. Moreover, the two hybridized portions on the polynucleotide target are separated by only 31 bases and are both near the gold substrate surface (Fig. 1). Consequently, in a small localized region, there is a high degree of steric congestion and electrostatic repulsion between the oligonucleotides on the gold nanoparticles (15) and the unhybridized probes, as well as the similar repulsive interactions between the oligonucleotides on the gold nanoparticles and the polynucleotide target (see Fig. 1). The probe/target/DNA-nanoparticle sandwich structure therefore adopts a surface orientation that will minimize all these interactions.

To further support our explanation of the AFM images based on the schematics, we performed contact angle measurements at the surfaces that had been examined by AFM. The contact angles determined with water droplets are 60° (at bare gold surface), 36° (at surface modified with only the probe), 40° (at surface covered with the probe–target complex), and 34° (at surface containing the probe–target–DNA/nanoparticle sandwich structures). The variation of the contact angles can be interpreted as follows. As the gold surface is modified with the probe molecules, the surface becomes more hydrophilic. After the polynucleotides have been hybridized at the surface, owing to the difference in the orientations between the tethered unhybridized probes and the flat-lying polynucleotides, the DNA film becomes somewhat disorganized (as opposed to the film containing only probes). Consequently, the contact angle increases slightly (i.e., 40°). The additional hybridization in Step 3 with the DNA on the nanoparticles causes the hybrid structure to tilt with respect to the underlying substrate surface. Because the hybrids become better organized and protrude above the unhybridized probe molecules on the surface (as demonstrated in Fig. 2d), solvation of these tethered macromolecules (37) decreases the contact angle to the smallest value (34°). The consistent trends between the change in the AFM images and the contact angle variation therefore provide useful microscopic and macroscopic insights into the surface orientation of the hybrids and the results arising from the two consecutive hybridization events.

CONCLUSION

Hybridization of oligonucleotides immobilized onto gold nanoparticles with the flat-lying polynucleotide molecules present at a gold substrate resulted in a dramatic change in the orientation of the probe–polynucleotide–DNA/nanoparticle sandwich structure. The sandwich structure adopts an orientation in which the polynucleotides become tethered to the surface with their strands protruding beyond the adjacent unhybridized probes. Such a rearrangement significantly improves the quality of AFM images, allowing a more accurate estimate of the surface density of the hybridized polynucleotide and the hybridization efficiency.

With the aid of DNA-capped nanoparticles, the hybridization efficiency was found to be about 16%. This is much greater than 1.1%, an underestimate based on the inclusion of only the resolvable polynucleotides prior to the interaction with the DNA-capped nanoparticles. The reorientation is probably driven by the necessity to reduce steric hindrance and electrostatic repulsion between the polynucleotide–DNA/nanoparticle adducts and the unhybridized probes. Through the second hybridization with the DNA-capped gold nanoparticles, we not only show that the procedure is useful in differentiating targets of similar sizes and base sequences (e.g., M13 mp18(+) vs M13 mp19(+)), but also confirm that the observed reorientation does not result from nonspecific adsorption of the DNA-capped gold nanoparticles. Finally, the agreement between the contact angle measurements and the AFM experiments at the various surfaces suggests that our proposed model is plausible in explaining the processes at such a heterogeneous DNA sensing surface from both macroscopic and microscopic viewpoints.

ACKNOWLEDGMENTS

Partial support for this work by a subproject in the NIH-MBRS/SCORE program, Donor of the Petroleum Research Funds, and the NSF-CRUI program (Grant DBI-9978806) is gratefully acknowledged.

REFERENCES

1. Watson, J., Gilman, M., Witkowski, J., and Zoller, M. (1992) Recombinant DNA, 2nd ed. Freeman, New York.
2. Chan, V., Graves, D. J., and McKenzie, S. E. (1995) *Biophys. J.* **69,** 2243–2255.
3. Steel, A. B., Herne, T. M., and Tarlov, M. J. (1998) *Anal. Chem.*, 4670–4677.
4. Peterlinz, K. A., Georgiadis, R. M., Herne, T. M., and Tarlov, M. J. (1997) *J. Am. Chem. Soc.* **119,** 3401–3402.
5. Hegner, M. D., M., Wagner, P., Semenza, G., and Guntherodt, J. J. (1996) *Microelectronics Nanometer Struct.* 1419–1421.
6. Levicky, R., Herne, T. M., Tarlov, M. J., and Satija, S. K. (1998) *J. Am. Chem. Soc.* **120,** 9787–9792.
7. Kelley, S. O., Barton, J. K., Jackson, N. M., and Hill, M. G. (1997) *Bioconjugate Chem.* **8,** 31–37.
8. Kelley, S. O., Barton, J. K., Jackson, N. M., McPherson, L. D., Porter, A. B., Spain, E. M., Allen, M. J., and Hill, M. G. (1998) *Langmui* **14,** 6781–6784.
9. Okahata, Y., Matsunobu, Y., Ijiro, K., Mukae, M., Murakami, A., and Makino, K. (1992) *J. Am. Chem. Soc.* **114,** 8299–8300.
10. Patolsky, F., Lichtenstein, A., and Willner, I. (2000) *J. Am. Chem. Soc.*, 418–419.
11. Takenaka, S. Y., K., Takagi, M., Uto, Y., and Kondo, H. (2000) *Anal. Chem.* **72,** 1334–1341.
12. Whittemore, N. A., Mullenix, A. N., Inamati, G. B., Manoharan, M., Cook, P. D., Tuinman, A. A., Baker, D. C., and Chambers, J. Q. (1999) *Bioconjugate Chem.* **10,** 261–270.
13. O'Brien, J. C., Stickney, J. T., and Porter, M. D. (2000) *J. Am. Chem. Soc.* **122,** in press.
14. Huang, E., Zhou, F., and Deng, L. (2000) *Langmuir* **16,** 3272–3280.
15. Demers, L. M., Mirkin, C. A., Mucic, R. C., Reynolds, R. A. I., Letsinger, R. L., Elgahanian, R., and Viswanadham, G. (2000) *Anal. Chem.* **72,** in press.
16. Taton, T. A., Mirkin, C. A., and Letsinger, R. L. (2000) *Science* **289,** 1757–1760.
17. Reynolds, R. A. I., Mirkin, C. A., and Letsinger, R. L. (2000) *J. Am. Chem. Soc.* **122,** in press.
18. Mirkin, C. A. (2000) *Inorg. Chem.* **39,** 2258–2272.
19. Mirkin, C. A., Letsinger, R. L., Nucic, R. C., and Storhoff, J. J. (1996) *Nature* **382,** 607–609.
20. Mirkin, M. A., Letsinger, R. L., Mucic, R. C., and Storhoff, J. J. (1997) *Biosensors Bioelectronics* **12,** 1–14.
21. Elghanian, R., Storhoff, J. L., Mucic, R. C., Letsinger, R. L., and Mirkin, C. A. (1997) *Science* **277,** 1078–1081.
22. Herne, T. M., and Tarlov, M. J. (1997) *J. Am. Chem. Soc.* **119,** 8916–8920.
23. Bamdad, C. (1998) *Biophys. J.* **75,** 1989–1996.
24. Storhoff, J. J., Elghanian, R., Mucic, R. C., Mirkin, C. A., and Letsinger, R. L. (1998) *J. Am. Chem. Soc.* **120,** 1959–1964.
25. Lin, L., Zhao, H.-Q., Li, J.-L., Tang, J.-A., Duan, M.-X., and Jiang, L. (2000) *Biochem. Biophys. Res. Commun.* **274,** 817–820.
26. Zhou, X.-C., O'Shea, J. S., and Li, S. F. Y. (2000) *Chem. Commun.*, 953–954.
27. He, L., Musick, M. D., Nicewarner, S. R., Salinas, F. G., Benkovic, S. J., Natan, M. J., and Keating, C. D. (2000) *J. Am. Chem. Soc.* **122,** 9070–9077.
28. Hansma, H. G., and Hoh, J. H. (1994) *Annu. Rev. Biomol. Struct.* **23,** 115–139.
29. Hansma, H. G., Sinsheimer, R. L., Groppe, J. C. B., Elings, V., Curley, G., Beznilla, M., Mastrangelo, I. A., Hough, P. V. C., and Hansma, P. K. (1993) *Scanning* **15,** 296–299.
30. Hayat, M. A. (1991) Colloidal Gold: Principles, Methods, and Applications, Academic Press, San Diego, CA.
31. Grabar, K. C., Freeman, R. G., Hommer, M. B., and Natan, M. J. (1995) *Anal. Chem.* **67,** 735–743.
32. Huang, E., Satiapipat, M., Han, S., and Zhou, F. (2000) Submitted.
33. Hansma, H. G., Kim, K. J., Laney, D. E., Garcia, R. A., Argaman, M., Allen, M. J., and Parsons, S. M. (1997) *J. Struct. Biol.* **119,** 99–108.
34. Magonov, S. N., and Whangbo, M.-H. (1996) Surface Analysis with STM and AFM, VCH/., and VCH Verlasgesllschaft, New York/Weinheim.
35. Wildrig, C. A., Alves, C. A., and Porter, M. D. (1991) *J. Am. Chem. Soc.* **113,** 2805–2810.
36. Lehninger, A. L., Nelson, D. L., and Cox, M. M. (1993) Principles of Biochemistry, Worth, New York.
37. Fawcett, N. C., Craven, R. D., Zhang, P., and Evans, J. A. (1998) *Anal. Chem.* **70,** 2876–2880.